AIAA SciTech Forum
23-27 January 2023, National Harbor, MD & Online
AIAA SCITECH 2023 Forum

10.2514/6.2023-1997

Data Fusion-Based Incremental Nonlinear Model Following Control Design for a Hypersonic Waverider Configuration

Johannes Autenrieb*
German Aerospace Center (DLR), Institute of Flight Systems, 38108 Braunschweig, Germany

The German Aerospace Center (DLR) investigates key technologies to implement hypersonic flight systems in various mission scenarios. In recent years, hypersonic glide vehicles (HGVs) received significant attention from academia and industry. HGV configurations can be used for civil and military purposes, operate over broad flight envelopes, and pose complex flight dynamic characteristics. This paper presents a hypersonic glide vehicle concept developed by DLR and gives a high-level overview on the established GNC system. Further, it proposes a data fusion-based nonlinear flight control architecture based on incremental nonlinear dynamic inversion, nonlinear model following control, and complementary filter theory. Since the considered vehicle possesses a redundant set of control effectors, an optimization-based control allocation approach is utilized to regulate the system dynamics. The proposed control architecture is first introduced and discussed. Later, robustness and performance investigations are conducted for validation purposes, using high-fidelity nonlinear flight dynamic simulations both in the nominal case and with model/sensor uncertainties. The acquired results indicate that the proposed strategy provides significant benefits for the robust nonlinear control of the hypersonic system.

I. Nomenclature

The notation convention used in this paper is widely based on the notation presented in the ISO 1151 standards series for flight mechanical quantities part one and two [1, 2].

Symbols

α	=	Angle of attack in rad
β	=	Side-slip angle in rad
C_i	=	Aerodynamic coefficient
χ	=	Flight path azimuth angle in rad
γ	=	Flight path angle in rad
H	=	Altitude in m
I	=	Moment of inertia in kgm^2
λ	=	Longitude in rad
L,M,N	=	External moments in the body axes in Nm
m	=	Mass in kg
Ma	=	Mach number
μ	=	Flight path bank angle in rad
ω	=	Natural frequency in rad/s
p,q,r	=	Roll, pitch, yaw rate in the body axes in rad/s
ϕ	=	Latitude in rad
ρ	=	Freestream density in kg/m^3
S	=	Aerodynamic reference area in m^2
u,v,w	=	Velocities in the body axes in m/s
V	=	Flight speed in m/s
X,Y,Z	=	External forces in the body axes in N
x,y,z	=	Distances in the body axes in m

*Research Scientist, Department of Flight Dynamics and Simulation.

ξ = Damping ratio

Subscripts

a = Aerodynamic frame
c = Command
cp = Centre of pressure
cg = Centre of gravity
K = Inertial frame
r = Reference

II. Introduction

In recent years, academic, industrial, and governmental organizations from all over the world have given increased attention to the development of hypersonic glide vehicles (HGVs). The German Aerospace Center (DLR) currently researches the performance and capabilities of autonomous HGVs in different mission scenarios. The design of robust guidance and control systems is mandatory for all autonomously operating flight vehicles. The mentioned systems are developed to regulate the vehicle's system dynamics and to enable it to correctly follow an online/offline computed trajectory to the desired location. Especially for the application in hypersonic vehicles, the developed flight control systems need to robustly operate in the presence of complex physical effects with fast-changing flight states and under the presence of model uncertainties and erroneous sensor information. Further difficulties arise from the fact that certain hypersonic configurations tend to have unstable open-loop behavior in the longitudinal motion and in the lateral-directional motion [3–5]. In combination with non-minimum phase characteristics, this can lead to a significant impact on closed-loop performance.

Most current control methodologies are designed using linearized models for which the nonlinear model is trimmed and linearized around selected operating points. To later control the overall nonlinear dynamics of the hypersonic vehicles, the control-relevant information of all considered operating points is connected with gain-scheduling approaches, such as proposed in Ref. [6]. However, to control the nonlinear system dynamics of hypersonic vehicles over the whole flight envelope, the procedure of trimming, linearization and gain-tuning need to be performed for all potential operating points. Employing this approach has the benefit that well-established analytical methodologies in the linear domain are used, and hence good predictions of the robustness properties of the vehicle can be given. Nevertheless, the development and validation of controllers for a broad set of operating points are often seen as laborious tasks for flight control designers. In recent years, nonlinear dynamic inversion (NDI) methodologies have gained popularity within the scientific community. Those approaches are capable of intrinsically handling the nonlinear system dynamics of hypersonic vehicles over the entire flight envelope based on a given mathematical model [7]. Hence, no gain scheduling is strictly required, even though it can also be used to modify the closed-loop behavior for changing operating points. Despite that major benefit, NDI-based control methods come also with drawbacks. In particular, NDI-methods can be sensitive to mathematical model uncertainties, which could lead to significant performance degradations and even closed-loop instabilities, due to inversion errors [8].

One control methodology that shows the ability to handle highly nonlinear systems more robustly is the incremental nonlinear dynamic inversion (INDI) control methodology. INDI has been successfully used and tested to control the flight dynamics of a broad set of aircraft systems. In Ref. [9] the authors successfully applied cascaded INDI feedback controllers for the attitude tracking and disturbance rejection of a spacecraft. In Ref. [10] researchers implemented and validated an INDI-based flight control system on a fixed-wing UAV successfully and showed its benefits over non-incremental methodologies. Even though the said approaches show promising results, both proposed control strategies rely on the implemented linear feedback controllers for good tracking performance and stability augmentation. Such a control structure makes it tedious to tune the controllers and consequently increases the possibility of high-gain solutions, tend to decreased robustness properties. Further, significant problems still need to be overcome when using incremental control strategies. Since the methodology relies on correct and instantaneous measurements of the angular acceleration and control effector states, the approach is exposed to instability problems if these sensed signals have significant noise, delays, and biases.

This paper proposes an incremental nonlinear model following control (INMFC) architecture, which increases the robustness against model and sensor uncertainties by enhancing a timescale-separated INDI control architecture with additional model-based knowledge. The paper's main contribution is the presentation and discussion of the INMFC flight control system, which combines cascaded and non-cascaded INDI-based control schemes to increase overall robustness by fundamentally separating the command tracking task from the stability augmentation task of the controllers. To further cope with problems related to erroneous sensor measurements, a complementary filter is proposed to fuse model-based information and sensor measurements, keeping the beneficial characteristics of both signals. After presenting and examining the overall proposed flight control architecture, the robustness and performance of the system are further analyzed using a simulation-based investigation.

The rest of the paper is structured in the following way. An overview of the vehicle and an overview of an exemplary mission design is given in Section III. In Section IV, the nonlinear mathematical model and relevant flight dynamic relationships are presented and discussed. The established nonlinear flight control system design is introduced and discussed in Section V. Finally, in Section VI, an example of a time simulation is used to demonstrate the control performance and the robustness of the proposed control system.

III. The DLR generic hypersonic glide vehicle 2 concept

Over the last years, DLR has worked on developing the generic hypersonic glide vehicle 2 (GHGV-2). The research project aims to investigate the capabilities and performance of strategic hypersonic glide vehicles and their impact on the perception of hypersonic threats [11].

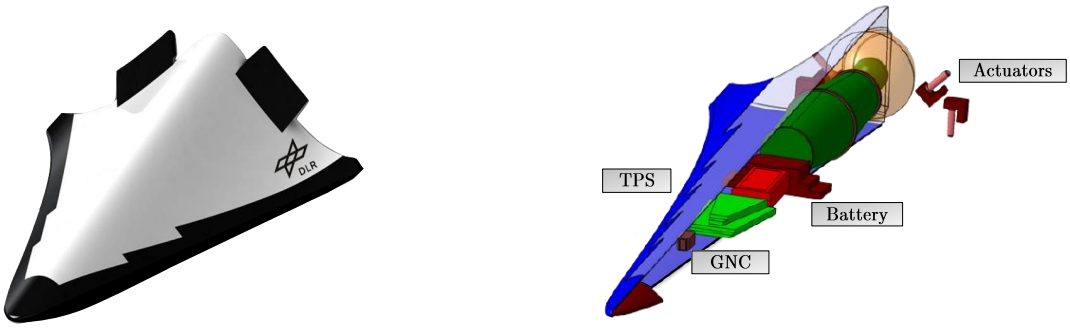

(a) External view on the GHGV-2 **(b) Sectional view of the GHGV-2**

Fig. 1 The DLR generic hypersonic glide vehicle concept 2 [12].

The developed vehicle is presented in Fig. 1a in an overall view and in Fig. 1b in a sectional view with relevant sub-systems, such as the thermal protection system (TPS), guidance, navigation & control system (GNC), battery, and actuators. The vehicle is designed as a waverider system, which has the aim of optimizing lift-to-drag ratios in high Mach number regimes [12]. While operating in endoatmospheric conditions, the vehicle uses four integrated flaps as control effectors to regulate the vehicle's attitude. In exoatmospheric conditions, small propulsors are integrated to generate the needed moments for changes in attitude. Since the flight control system aims to exclusively control the vehicle's attitude, and considering the number of redundant control effectors in both flight phases, the vehicle is considered over-actuated. In such a case, the application of suitable control allocation algorithms is needed.

Fig. 2 compares two altitude trajectories for a classical ballistic missile system (given in blue) and an HGV (given in red) during a exemplary mission. Both vehicles launch from an Earth-based launch site using boost rockets. After the ignition and acceleration phase of the rockets, the HGV system decouples from the head section of the launch vehicle at an altitude of approximately 100 km and initiates a re-entry phase. In comparison, the ballistic missile system rises to an altitude of approximately 300 km before re-entering. After the parabolic re-entry phase of the HGV, the system enters the atmospheric glide phase at an altitude of approximately 40 km. This phase takes up most of the mission time. During the atmospheric glide phase, the vehicle tries to maintain the $(L/D)_{max}$ related flight path angle γ, while flying towards its target. Fig. 2 indicates that HGVs are more challenging to identify and track by earth-based radar systems

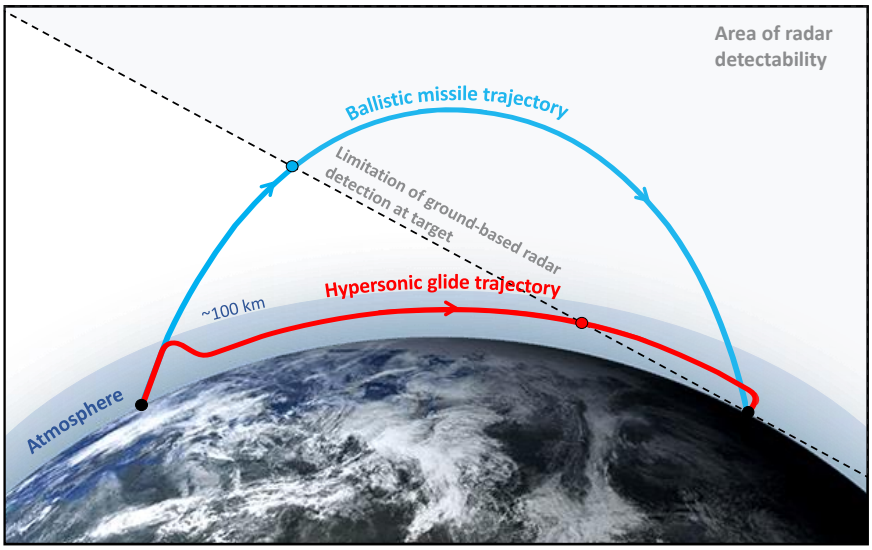

Fig. 2 Missions examples and comparisions of HGV and classical ballistic missile systems[11].

compared to commonly used ballistic missile systems. Due to the tangential spreading of the electromagnetic radiation, relative to the Earth's surface, the lower-flying HGV systems are, in general, later detectable than higher-flying ballistic missile systems, leading to significantly shorter reaction times for defense infrastructures. A further challenge is that HGVs, compared to classical ballistic systems, possess higher maneuverability within the atmosphere, which leads to enormous challenges for defense architectures predicting their future trajectories and targets during the glide phase.

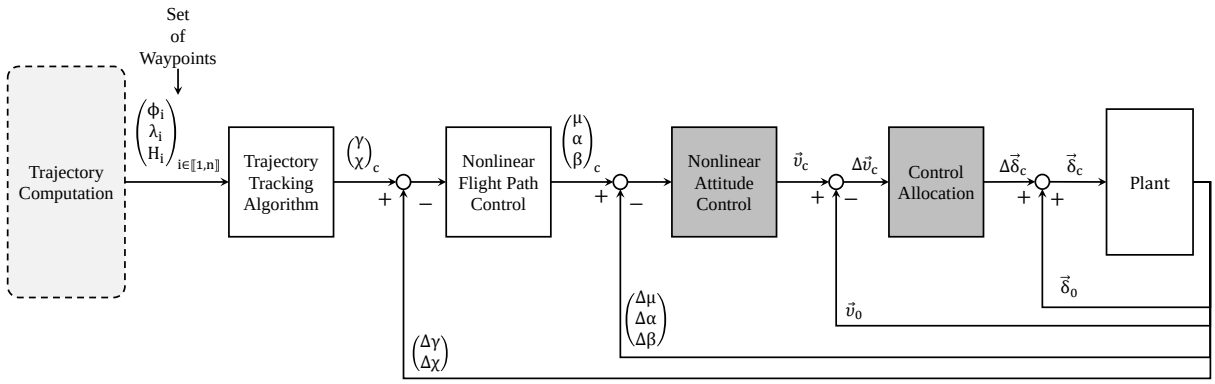

Fig. 3 Overview of the integrated overall guidance and control architecture of the GHGV-2.

Fig. 3 shows a conceptual architecture of the overall guidance and control system of the GHGV-2. In the first step, the trajectory for the vehicle needs to be computed, e.g., using optimization-based approaches such as shown in Ref. [13]. These trajectories must be computed so that the vehicle's physical (e.g., thermal loads) and operational constraints (e.g., no-fly zones) are not violated. After a suitable trajectory, in the form of a set of position waypoints (latitude ϕ, longitude λ and altitude H), is obtained, a trajectory tracking algorithm uses the vehicle's current position and the waypoint information to compute the currently required flight path angles (χ_c, γ_c). These demanded flight angles are then fed into an NDI-based flight path controller that generates the required aerodynamic angles $(\mu_c, \alpha_c, \beta_c)$, later used by the nonlinear attitude control system. This generates a virtual control command vector $\vec{\nu} = (\dot{p}_c, \dot{q}_c, \dot{r}_c)^T$, which is then incrementalized as $\Delta\vec{\nu}$. The incremental virtual control command vector $\Delta\vec{\nu}$ is then fed into a control allocation system to compute the incremental control input vector $\Delta\vec{\delta}_c$, which is later augmented with the measured control input vector $\vec{\delta}_0$ before using it to command the vehicle. Even though all presented sub-modules have a substantial internal dependency on each other, the discussions within the work presented here will exclusively focus on the "nonlinear attitude control" and "control allocation" modules.

IV. Flight dynamics simulation

The nonlinear simulation model of the developed GHGV-2 was developed together with colleagues from the DLR Institute of Aerodynamics and Flow Technology. The simulation is programmed in a MATLAB/Simulink environment and focuses specifically on the development of control systems for hypersonic flight vehicles; see [11] for more details. In the following section, the aerodynamic modeling of the considered vehicle and relevant aspects of the flight mechanics of hypersonic vehicles are briefly introduced and discussed.

A. Aerodynamics

In the current state, the aerodynamic database considers static and dynamic aerodynamical effects modeled as static and dynamic derivative coefficients. Each of the coefficients is a function of the Mach number Ma, the altitude H, the angle of attack α and the angle of sideslip β (see Eq. 1- 6).

$$X = \frac{\rho}{2}V^2 S[C_X(\alpha,\beta,\mathrm{Ma},\mathrm{H}) + C_{X,q}(\alpha,\beta,\mathrm{Ma},\mathrm{H})\frac{ql_r}{2V}] \tag{1}$$

$$Y = \frac{\rho}{2}V^2 S[C_Y(\alpha,\beta,\mathrm{Ma},\mathrm{H}) + C_{Y,r}(\alpha,\beta,\mathrm{Ma},\mathrm{H})\frac{rl_r}{2V}] + C_{Y\dot{\beta}}(\alpha,\beta,\mathrm{Ma},\mathrm{H})\frac{\dot{\beta}l_r}{2V}] \tag{2}$$

$$Z = \frac{\rho}{2}V^2 S[C_Z(\alpha,\beta,\mathrm{Ma},\mathrm{H}) + C_{Z,q}(\alpha,\beta,\mathrm{Ma},\mathrm{H})\frac{ql_r}{2V} + C_{Z,\dot{\alpha}}(\alpha,\beta,\mathrm{Ma},\mathrm{H})\frac{\dot{\alpha}l_r}{2V}] \tag{3}$$

$$L = \frac{\rho}{2}V^2 S[C_l(\alpha,\beta,\mathrm{Ma},\mathrm{H}) + C_{l,p}(\alpha,\beta,\mathrm{Ma},\mathrm{H})\frac{ql_r}{2V}] - Y\Delta z_{cp-cg} - Z\Delta y_{cp-cg} \tag{4}$$

$$M = \frac{\rho}{2}V^2 S[C_M(\alpha,\beta,\mathrm{Ma},\mathrm{H}) + C_{M,q}(\alpha,\beta,\mathrm{Ma},\mathrm{H})\frac{ql_r}{2V} + C_{M\dot{\alpha}}(\alpha,\beta,\mathrm{Ma},\mathrm{H})\frac{\dot{\alpha}l_r}{2V}] - Z\Delta x_{cp-cg} + X\Delta z_{cp-cg} \tag{5}$$

$$N = \frac{\rho}{2}V^2 S[C_N(\alpha,\beta,\mathrm{Ma},\mathrm{H}) + C_{N,r}(\alpha,\beta,\mathrm{Ma},\mathrm{H})\frac{rl_r}{2V} + C_{N,\dot{\beta}}(\alpha,\beta,\mathrm{Ma},\mathrm{H})\frac{\dot{\beta}l_r}{2V}] + X\Delta y_{cp-cg} + Y\Delta x_{cp-cg} \tag{6}$$

The static aerodynamic coefficients have been calculated by computational fluid dynamics (CFD) with the DLR TAU code [14, 15]. For the CFD analysis, roughly 800 inviscid calculations were performed for different Mach numbers, angles of attack, angles of sideslip, and rudder deflection angle combinations. Viscosity effects are accounted for by performing fully viscous Reynolds-Averaged Navier-Stokes simulations for selected trajectory points. For simplicity, within the flight dynamical model used here, the control effectiveness of the control surfaces is assumed to be linear, leading to a control affine dynamical system.

B. Flight mechanics

The modeled GHGV-2 is assumed to be a rigid body, and the nonlinear flight dynamics of the HGV are based on classical Newtonian mechanics. Fig. 4 displays the components X, Y, Z of the total external force vector $\vec{R}$ and the components L, M, N of the total external moment vector $\vec{Q}$ expressed in the body-fixed frame of the vehicle. Since the presented work mainly focuses on the unpropelled re-entry and atmospheric glide phase, only the aerodynamic and gravitational forces and moments are considered.

Eq. (7) and Eq. (8) present the generalized equations of motion of a flight vehicle for the translational and the rotational movement.

$$\vec{R} = \begin{bmatrix} X \\ Y \\ Z \end{bmatrix} = m \begin{bmatrix} \dot{u}_K \\ \dot{v}_K \\ \dot{w}_K \end{bmatrix} + m \begin{bmatrix} p_K \\ q_K \\ r_K \end{bmatrix} \times \begin{bmatrix} u_K \\ v_K \\ w_K \end{bmatrix} \tag{7}$$

$$\vec{Q} = \begin{bmatrix} L \\ M \\ N \end{bmatrix} = I \begin{bmatrix} \dot{p}_K \\ \dot{q}_K \\ \dot{r}_K \end{bmatrix} + \begin{bmatrix} p_K \\ q_K \\ r_K \end{bmatrix} \times I \begin{bmatrix} p_K \\ q_K \\ r_K \end{bmatrix} \tag{8}$$

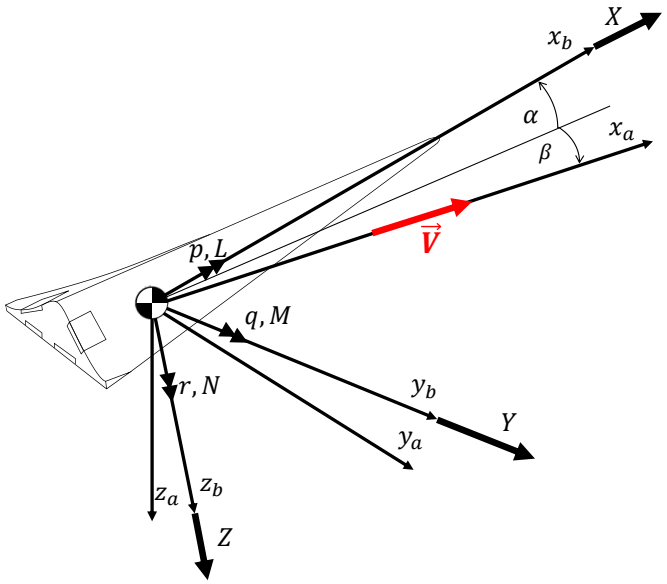

Fig. 4 Sketch of external forces and moments acting on the GHGV-2 concept [11] .

An important kinematic relationship, here described in the inertial axes denoted by the index K, that connects the time derivatives of the flight-path bank angle μ_K, the angle of attack α_K and the sideslip angle β_K to the body-fixed rotational rates p_K, q_K, r_K and the corresponding time derivatives of the flight path angle γ and χ can be stated as [16]:

$$\begin{aligned}\begin{bmatrix}\dot{\mu}_K\\ \dot{\alpha}_K\\ \dot{\beta}_K\end{bmatrix} = T_1\begin{bmatrix}p_K\\ q_K\\ r_K\end{bmatrix} + T_2\begin{bmatrix}\dot{\gamma}\\ \dot{\chi}\end{bmatrix} &= \begin{bmatrix}\frac{\cos\alpha_K}{\cos\beta_K} & 0 & \frac{\sin\alpha_K}{\cos\beta_K}\\ -\cos\alpha_K\tan\beta_K & 1 & -\sin\alpha_K\tan\beta_K\\ \sin\alpha_K & 0 & -\cos\alpha_K\end{bmatrix}\begin{bmatrix}p_K\\ q_K\\ r_K\end{bmatrix}\\ &+\begin{bmatrix}\cos\mu_K\tan\beta_K & \sin\gamma+\sin\mu\tan\beta_K\cos\gamma\\ -\frac{\cos\mu_K}{\cos\beta_K} & -\frac{\sin\mu_K\cos\gamma}{\cos\beta_K}\\ -\sin\mu_K & \cos\mu_K\cos\gamma\end{bmatrix}\begin{bmatrix}\dot{\gamma}\\ \dot{\chi}\end{bmatrix}\end{aligned} \tag{9}$$

The influence of $\dot{\gamma}$ and $\dot{\chi}$ on the prior equation can alternatively be expressed as functions of the externally acting weight force W, aerodynamic lift force L_A and aerodynamic side force Y_A described in the inertial axes [17]:

$$\begin{aligned}\begin{bmatrix}\dot{\mu}_K\\ \dot{\alpha}_K\\ \dot{\beta}_K\end{bmatrix} = T_1\begin{bmatrix}p_K\\ q_K\\ r_K\end{bmatrix} + \left(\frac{1}{mV}\right)T_3\begin{bmatrix}-W\\ L_A\\ Y_A\end{bmatrix} &= \begin{bmatrix}\frac{\cos\alpha_K}{\cos\beta_K} & 0 & \frac{\sin\alpha_K}{\cos\beta_K}\\ -\cos\alpha_K\tan\beta_K & 1 & -\sin\alpha_K\tan\beta_K\\ \sin\alpha_K & 0 & -\cos\alpha_K\end{bmatrix}\begin{bmatrix}p_K\\ q_K\\ r_K\end{bmatrix}\\ &+\left(\frac{1}{mV}\right)\begin{bmatrix}\cos\gamma\cos\mu_K\tan\beta_K & \tan\gamma\sin\mu_K+\tan\beta_K & \tan\gamma\cos\mu_K\cos\beta_K\\ \frac{\cos\gamma\cos\mu_K}{\cos\beta_K} & -\frac{1}{\cos\beta_K} & 0\\ \cos\gamma\sin\mu_K & 0 & \cos\beta_K\cos\gamma\end{bmatrix}\begin{bmatrix}-W\\ L_A\\ Y_A\end{bmatrix}\end{aligned} \tag{10}$$

Both equations Eq. (9) and Eq. (10) can also describe the dynamics of the considered flight vehicle during operations in windy conditions. However, to simplify the notation for this paper, the absence of wind is assumed. In that case, the inertial axes denoted by the index K correspond with the aerodynamic axes denoted by the index a. This simplifies the notation during the rest of the paper, describing the body-rate rate vector in the inertial axes, denoted by the index K, without the corresponding index. The discussed assumptions and simplifications lead to the subsequent notation:

$$\begin{bmatrix}\mu_K\\ \alpha_K\\ \beta_K\end{bmatrix} = \begin{bmatrix}\mu_a\\ \alpha_a\\ \beta_a\end{bmatrix} = \begin{bmatrix}\mu\\ \alpha\\ \beta\end{bmatrix} \tag{11}$$

$$\begin{bmatrix}\gamma_a\\ \chi_a\end{bmatrix} = \begin{bmatrix}\gamma\\ \chi\end{bmatrix} \tag{12}$$

$$\begin{bmatrix}p_K\\ q_K\\ r_K\end{bmatrix} = \begin{bmatrix}p\\ q\\ r\end{bmatrix} \tag{13}$$

The lift force L_A and the side force Y_A are computed based on the aerodynamic database presented in Sect. 6.

V. Data fusion-based incremental nonlinear model following control

For the here considered GHGV-2, a data-fusion-based incremental nonlinear model-following-control system was designed and integrated. The work presented here is building on prior research activities, discussed in Ref. [18], where a non-incremental NMFC solution for the attitude control problem of the GHGV-2 was presented. The overall flight control architecture of the proposed control architecture is shown in Fig. 5.

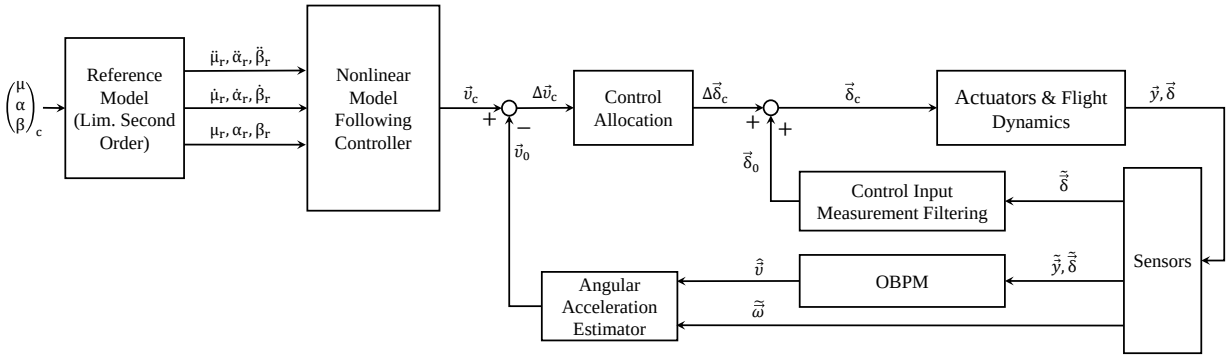

Fig. 5 Overview on proposed data-fusion-based nonlinear model-following-control system architecture for the GHGV-2.

The architecture uses a second-order reference model (RM) system to filter the command input vector $(\mu_c, \alpha_c, \beta_c)^T$ and shape the desired reference signal vector $(\mu_r, \alpha_r, \beta_r)^T$. The generated reference signals are the filtered commands and the corresponding first- and second-time derivatives of the desired model response. A nonlinear model following control system uses the provided information on the different time scales to control the system as desired. The controllers generate a virtual control command vector $\vec{\nu}_c$ which holds the information about the needed angular acceleration $(\dot{p}_c, \dot{q}_c, \dot{r}_c)^T$ in the body-fixed frame. This information is then incremented by subtracting an estimate of the current angular acceleration of the vehicle obtained with a complementary filter, which merges the sensor-based information with estimated behavior coming from an onboard plant model (OBPM). The incremental virtual control command $\Delta\vec{\nu}_c$ is used by an optimization-based control allocation approach to compute the control deflection vector $\Delta\vec{\delta}_c$, while respecting limits on the actuators. Afterward, the signal is augmented with the low-pass filtered and synchronized measurement of the control surface deflection vector $\tilde{\vec{\delta}}_0$. In the following section, all of the briefly illustrated modules are further described and discussed in-depth.

A. Reference model

The RM is used to low-pass filter the command inputs and shape the desired reference signals. The reference model incorporates further knowledge of limitations on the time scales of the commanded states and protects the controllers of unreachable reference signals. The defined limits on the different time scales can, for example, originate from limits on the structural or thermal loads that the vehicle should not exceed. Further, limitations based on the attainable moment of the control effectors over changing operating points can be considered in the limitation of the modeled reference behavior. As long as the system is operating within its defined boundaries, each incoming command from the guidance system $(\mu_c, \alpha_c, \beta_c)^T$ is shaped by a second-order transfer function of the following form:

$$G_r(s) = \frac{\omega_r^2}{s^2 + 2D_r\omega_r s + \omega_r^2} \tag{14}$$

The eigenfrequency ω_r and the damping ratio D_r of the presented transfer function can be chosen such that the desired system response behavior can be imposed on the vehicle. D_r is often chosen to be 0.707 to get a small pitch-rate overshoot and short settling time [19]. In the context of high-performance systems, ω_r is chosen depending on the eigenfrequency of the dominant open-loop dynamics. Besides the desired low-pass filtered reference signal for the aerodynamic angles, the reference model also generate the desired response's first- and second-order derivatives. Fig. 6 shows all signals generated by the RM and how the proposed INMFC control system uses them.

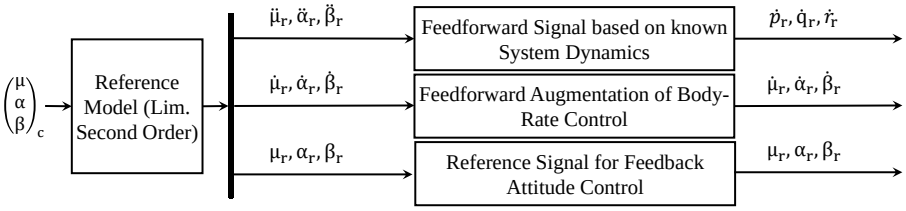

Fig. 6 Conceptual illustration of the generated signals of the reference model and their use in the INMFC.

The two higher-order reference signals ($(\dot{\mu}_r, \dot{\alpha}_r, \dot{\beta}_r)^T$ and $(\ddot{\mu}_r, \ddot{\alpha}_r, \ddot{\beta}_r)^T$) are used as feedforward control signals. The first signal is directly as a reference signal to the inner-loop controller (further discussed in V.B.1), while the other is used to compute a reference virtual control command via an NDI-based transformation (further discussed in V.B.2). The low-pass filtered reference signal is used in the outer-loop feedback controller to regulate the error terms of the aerodynamical angles $(\mu_r, \alpha_r, \beta_r)^T$.

B. Incremental nonlinear model-following-control design

Fig. 7 shows the integrated INMFC architecture. Using the proposed data fusion-based nonlinear control methodology allows a partial decomposition of the tracking and regulation of the controlled states by combining cascaded and non-cascaded NDI-based approaches.

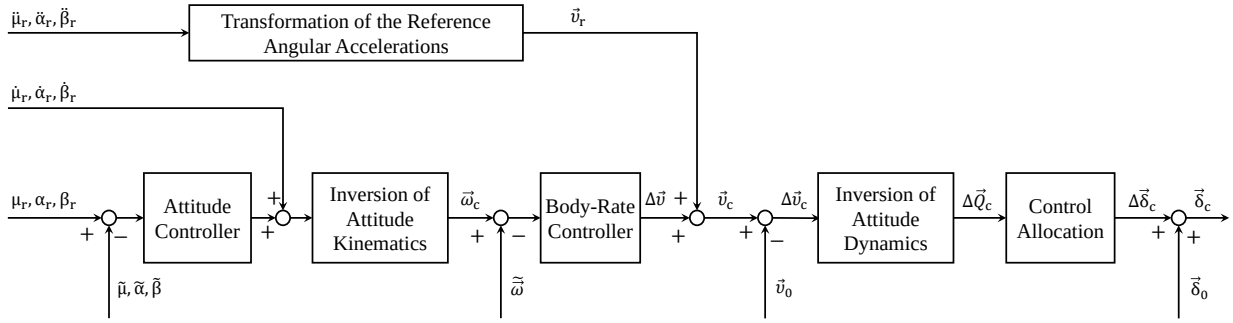

Fig. 7 Overview on proposed incremental nonlinear model following control architecture for the GHGV-2.

The central part of the tracking task is taken over by transforming the computed higher-order derivatives of the feedforward signals based on known reference dynamics and system kinematics via a non-cascaded NDI methodology. The regulation of the vehicle dynamics is addressed by using a nonlinear control feedback path to handle uncertainties and external disturbances. For the feedback control, a cascaded time-scale separated nonlinear dynamic inversion control system is implemented. Employing the proposed combined (cascaded and non-cascaded) nonlinear control approach eases the tuning of the feedback gains (by only concentrating on stability augmentation and disturbance rejection requirements) and consequently decreases the risk of high-gain solutions, which could lead to decreased robustness properties.

1. Time-scale separated NDI feedback control design

A cascaded nonlinear dynamic inversion feedback controller, with distinct linear controllers for the attitude and body-rate control, is implemented for good stability augmentation and disturbance rejection capabilities of the vehicle. The integrated cascaded feedback control approach is based on the idea of time-scale separated nonlinear dynamic inversion systems. The developed NDI feedback control system is similar to the feedback control architectures proposed in Ref. [17] and Ref. [7], but is adapted to match the characteristics of the controlled GHGV-2. In the following, the implementation of the feedback control system is introduced and discussed.

The linear outer-loop controller computes the needed $(\Delta\dot{\mu}, \Delta\dot{\alpha}, \Delta\dot{\beta})^T$ based on the attitude error vector $(e_\mu, e_\alpha, e_\beta)^T$, which is computed based on the state measurements $(\tilde{\mu}, \tilde{\alpha}, \tilde{\beta})^T$ and the obtained low-pass filtered reference signals $(\mu_r, \alpha_r, \beta_r)^T$ of the RM.

$$\begin{bmatrix} \Delta\dot{\mu} \\ \Delta\dot{\alpha} \\ \Delta\dot{\beta} \end{bmatrix} = K_{\mu\alpha\beta} \begin{bmatrix} e_\mu \\ e_\alpha \\ e_\beta \end{bmatrix} = \begin{bmatrix} K_\mu & 0 & 0 \\ 0 & K_\alpha & 0 \\ 0 & 0 & K_\beta \end{bmatrix} \left(\begin{bmatrix} \mu_r \\ \alpha_r \\ \beta_r \end{bmatrix} - \begin{bmatrix} \tilde{\mu} \\ \tilde{\alpha} \\ \tilde{\beta} \end{bmatrix} \right) \tag{15}$$

The overall commanded first-order time derivatives of the aerodynamic angles are received by combining the first-order reference model signal vector $(\dot{\mu}_r, \dot{\alpha}_r, \dot{\beta}_r)^T$ and the feedback control signal vector $(\Delta\dot{\mu}, \Delta\dot{\alpha}, \Delta\dot{\beta})^T$:

$$\begin{bmatrix} \dot{\mu}_c \\ \dot{\alpha}_c \\ \dot{\beta}_c \end{bmatrix} = \begin{bmatrix} \dot{\mu}_r \\ \dot{\alpha}_r \\ \dot{\beta}_r \end{bmatrix} + \begin{bmatrix} \Delta\dot{\mu} \\ \Delta\dot{\alpha} \\ \Delta\dot{\beta} \end{bmatrix} \tag{16}$$

Based on the kinematic relationship presented in Eq. (15) the commanded signal vector $(\Delta\dot{\mu}, \Delta\dot{\alpha}, \Delta\dot{\beta})^T$ can be transformed into a reference body-rate signal $(p_c, q_c, r_c)^T$ for the inner-loop controller with the following inversion law:

$$\vec{\omega}_c = \begin{bmatrix} p_c \\ q_c \\ r_c \end{bmatrix} = T_1^{-1} \left(\begin{bmatrix} \dot{\mu}_c \\ \dot{\alpha}_c \\ \dot{\beta}_c \end{bmatrix} - \left(\frac{1}{mV} \right) T_3 \begin{bmatrix} -W \\ L_A \\ Y_A \end{bmatrix} \right) \tag{17}$$

The linear inner-loop controller calculates the corrective virtual control commands $(\Delta\dot{p}, \Delta\dot{q}, \Delta\dot{r})^T$ needed to eliminate the rate control error based on the rate error vector $(e_p, e_q, e_r)^T$, which is computed using the body-rate state measurements $(\tilde{p}, \tilde{q}, \tilde{r})^T$ and the obtained reference signals from the prior angular kinematics inversion step:

$$\Delta\vec{\nu} = \begin{bmatrix} \Delta\dot{p} \\ \Delta\dot{q} \\ \Delta\dot{r} \end{bmatrix} = K_{pqr} \begin{bmatrix} e_p \\ e_q \\ e_r \end{bmatrix} = \begin{bmatrix} K_p & 0 & 0 \\ 0 & K_q & 0 \\ 0 & 0 & K_r \end{bmatrix} \left(\begin{bmatrix} p_c \\ q_c \\ r_c \end{bmatrix} - \begin{bmatrix} \tilde{p} \\ \tilde{q} \\ \tilde{r} \end{bmatrix} \right) \tag{18}$$

2. NDI-based feedforward control signal generation

The second-order time derivative vector $(\ddot{\mu}_r, \ddot{\alpha}_r, \ddot{\beta}_r)^T$ of the shaped reference response, generated by the RM, is used for feedforward purposes by using the known kinematic relationship presented in Eq. (9). Following the NDI methodology, the regarded dynamic relationship needs to be further derived to obtain the needed input-output connection with a relative degree of two, which matches the second-order derivatives of the reference signal vector with the feedforwarded virtual control command vector $(\dot{p}_r, \dot{q}_r, \dot{r}_r)^T$ [16]. The final feedforward virtual control command signal is described as:

$$\vec{\nu}_r = \begin{bmatrix} \dot{p}_r \\ \dot{q}_r \\ \dot{r}_r \end{bmatrix} = T_1^{-1} \left[\begin{pmatrix} \ddot{\mu}_r \\ \ddot{\alpha}_r \\ \ddot{\beta}_r \end{pmatrix} - \dot{T}_1 \begin{pmatrix} \tilde{p} \\ \tilde{q} \\ \tilde{r} \end{pmatrix} - \dot{T}_2 \begin{pmatrix} \dot{\tilde{\gamma}} \\ \dot{\tilde{\chi}} \end{pmatrix} - T_2 \begin{pmatrix} \ddot{\tilde{\gamma}} \\ \ddot{\tilde{\chi}} \end{pmatrix} \right] \tag{19}$$

The overall virtual control command vector (angular acceleration command) is obtained by combining the transformed second-order reference model signal vector $(\dot{p}_r, \dot{q}_r, \dot{r}_r)^T$ and the feedback control signal vector $(\Delta\dot{p}, \Delta\dot{q}, \Delta\dot{r})^T$:

$$\vec{\nu}_c = \begin{bmatrix} \dot{p}_c \\ \dot{q}_c \\ \dot{r}_c \end{bmatrix} = \vec{\nu}_r + \Delta\vec{\nu} = \begin{bmatrix} \dot{p}_r \\ \dot{q}_r \\ \dot{r}_r \end{bmatrix} + \begin{bmatrix} \Delta\dot{p} \\ \Delta\dot{q} \\ \Delta\dot{r} \end{bmatrix} \tag{20}$$

3. Incrementalization of the virtual control command vector

To minimize the model dependencies and reduce the vulnerability of the integrated model-based nonlinear control methodology, an INDI-based approach is applied to the control problem. The application of the methodology aims to reduce needed model information by substituting parts of the needed model information with sensed/estimated data in order to prevent inversion errors, and possible destabilization of the controller due to a model mismatch [9]. In order to apply the incremental control strategy to the given problem, the computed overall virtual control command vector $\vec{\nu}_c$ is incrementalized with the estimated currently acting virtual control command $\vec{\nu}_0$:

$$\Delta\vec{\nu}_c = \vec{\nu}_c - \vec{\nu}_0 \tag{21}$$

The required incremental moment vector is computed by inverting the differential equation given in Eq. 8:

$$\Delta\vec{Q}_c = \begin{bmatrix} \Delta L_c \\ \Delta M_c \\ \Delta N_c \end{bmatrix} = I \begin{bmatrix} \Delta\dot{p}_c \\ \Delta\dot{q}_c \\ \Delta\dot{r}_c \end{bmatrix} + \begin{bmatrix} \tilde{p} \\ \tilde{q} \\ \tilde{r} \end{bmatrix} \times I \begin{bmatrix} \tilde{p} \\ \tilde{q} \\ \tilde{r} \end{bmatrix} \tag{22}$$

The incremental moment vector is then fed into the control allocation, which then computes the new incremental control input vector $\Delta\vec{\delta}_c$. To finally generate a valid control input command, the computed incremental control input vector is later combined with the estimated current command input vector $\vec{\delta}_0$:

$$\vec{\delta} = \vec{\delta}_0 + \Delta\vec{\delta}_c \tag{23}$$

C. Sensor filtering and estimation

As emphasized previously, applying an incremental control strategy can minimize the vulnerability of the model-based nonlinear control methodology toward model uncertainties. However, if applied to the attitude control of aerial vehicles, it increases the need for accurate measurements of the angular accelerations $(\dot{p}, \dot{q}, \dot{r})^T$, which are often not directly measurable. In cases where the control methodology is applied on less maneuverable or small aircraft, such as passenger aircraft or fixed-wing UAVs, filtering and differentiating the measured body rates is a practical approach which shows good results, as presented in Ref. [20] and Ref. [10]. In cases involving a highly maneuverable system, for which large and rapid changes in the angular accelerations are expected such an approach could lead to significant troubles. A phase lag with respect the actual acceleration (due to the numerical differentiation of the current body rates and the additional low-pass filtering) as well as sensor delays/noise properties could corrupt the flight control system's overall control performance and robustness. An alternative approach would be to predict the instantaneous angular acceleration of the vehicle purely using an OBPM, which would allow the angular acceleration information to be obtained with neglectable phase lags. On the other hand, this approach again exposes the flight control system to problems related to poorly known vehicle models and unmeasurable disturbances.

A technique that is able to bring the complementary benefits of both approaches together is based on complementary filter (CF) theory. By using a CF-based estimation strategy, the fast and less noisy, but potentially inaccurate, model-based prediction can be fused with the sensor information, which can measure the actual value but might have significant noise and phase lag [21]. In general, a CF can be interpreted as a steady-state Kalman filter. However, compared to a classical Kalman filter, a complementary filter needs less information about the noise's statistical characteristics, which leads to a more straightforward structure and decreased computational costs [22].

Using a CF-based estimation method can also have benefits for estimating the current control input state, which is used to augment the incremental control input command coming from the control allocation. Even though prior research activities, as shared in Ref. [9], have shown that noisy and delayed sensing of the actual control inputs often has no significant influence on the overall control performance/robustness of an INDI-based control system, it was remarked in Ref. [9] that for cases with highly nonlinear actuator properties, a data-fusion-based estimation could be benefical [9]. However, experimental analyses on the considered vehicle have shown that well designed low-pass and

synchronization filter for the control input measurements are sufficient enough for a robust incremental control of the vehicle. Comparison studies with an CF-based control input estimator approach showed no significant benefits, hence it was decided to not implement a CF-based control input estimation. In the following, the integrated approach for the complementary filter-based estimation of the angular acceleration vector $\vec{\nu}_0$ and the low-pass and synchronization filtering of the control input vector $\vec{\delta}_0$ is presented and discussed.

1. Complementary filter-based angular acceleration estimation

The overall architecture of the complementary filter for the angular acceleration is shown in Fig. 8 and is similar to the complementary filter proposed by Jiali et al. presented in Ref. [21] for the estimation of angular accelerations.

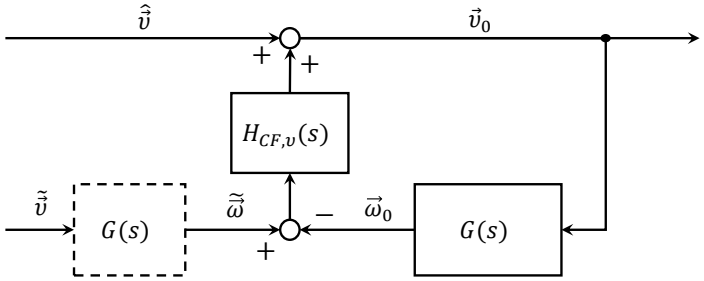

Fig. 8 Conceptual design of complementary filter for the angular acceleration estimation.

where $G(s)$ is an integrator in the continuous-time domain, $\vec{\omega}_0$ is the data fusion-based body-rate estimation, computed by integrating the estimated angular acceleration vector $\vec{\nu}_0$, and $\tilde{\vec{\omega}}$ is the sensed body-rate signal in the body-fixed frame coming from the IMU. The model-based angular acceleration estimation $\hat{\vec{\nu}}$ is computed using an OBPM that is based on the aerodynamic database presented in Sect. IV.A. The overall estimation signal can be defined as:

$$\begin{aligned}\vec{\nu}_0 &= \frac{1}{1+G(s)H_{CF,\nu}(s)}\hat{\vec{\nu}} + \frac{H_{CF,\nu}(s)G(s)}{1+G(s)H_{CF,\nu}(s)}\tilde{\vec{\nu}} \\ &= \frac{1}{1+G(s)H_{CF,\nu}(s)}\hat{\vec{\nu}} + \frac{H_{CF,\nu}(s)}{1+G(s)H_{CF,\nu}(s)}\tilde{\vec{\omega}}\end{aligned} \tag{24}$$

with $H_{CF,\nu}$ chosen to be a proportional-integral control in the following form:

$$H_{CF,\nu}(s) = K_p + \frac{K_i}{s} \tag{25}$$

with K_p being the proportional gain and K_I the integral gain, both tuned to ensure a good convergence with the true value, while suppressing sensor noise and mitigating time delay related problems. This leads to the following overall equation for the estimation:

$$\vec{\nu}_0 = \frac{s^2}{s^2 + K_p s + K_I}\hat{\vec{\nu}} + \frac{K_p s + K_I}{s^2 + K_p s + K_I}\tilde{\vec{\omega}} \tag{26}$$

The natural frequency $\omega_{CF,\nu}$ and the damping ratio $\xi_{CF,\nu}$ of the established second-order filter can be computed as follows:

$$\omega_{CF,\nu} = \sqrt{K_I} \tag{27}$$

$$\xi_{CF,\nu} = \frac{K_p}{2\sqrt{K_I}} \tag{28}$$

The derivation shows the complementary nature of the approach in which the overall equation can be interpreted as:

$$\vec{\nu}_0 = T(s)\hat{\vec{\nu}} + S(s)\tilde{\vec{\omega}} \tag{29}$$

where $T(s)$ is a low-pass filter for the model-based angular acceleration prediction $\hat{\vec{\nu}}$ and $S(s)$ is a high-pass filter for the measured body-rate vector $\tilde{\vec{\omega}}$. Both filters can be specifically tuned to keep desired high-frequency properties and to mitigate low-frequency uncertainties of the model-based prediction, and to low-pass filter sensor signals that are afflicted with high-frequency noise. By respecting $T(s) + S(s) = 1$, it can be ensured that the cut-off frequencies for both filters are the same.

2. Low-pass and synchronization filtering of control input signals

For the computation of the control surface deflection vector $\vec{\delta}_0$, no complementary filter was used and the raw control surface information was filtered by an low-pass filter and a synchronization filter, in the following form:

$$\vec{\delta}_0 = H_f(s)H_{sync}(s)\tilde{\vec{\delta}} \tag{30}$$

with $\tilde{\vec{\delta}}$ being the sensed control surface deflection vector, $H_f(s)$ the transfer function of the low-pass filter in the continuous time domain and $H_{sync}(s)$ the transfer function of the synchronization filter in the continous time domain. The low-pass filter transfer function $H_f(s)$ was, as suggested in Ref. [20], chosen to be a second-order low-pass filter in the form of:

$$H_f(s) = \frac{\omega_f^2}{s^2 + 2D_f\omega_f s + \omega_f^2} \tag{31}$$

The researchers in Ref. [23] and in Ref. [20] suggested that a synchronization filter, defined as $H_{sync}(s)$, is additionally required for an effective incremental control approach. The first order lag $H_{sync}(s)$ is used for the synchronization between the sensed control deflection and angular acceleration signals. This is done by adding an additional time delay to the leading sensed raw control input vector $\tilde{\vec{\delta}}$ in the following form:

$$H_{sync}(s) = \frac{1}{t_s s + 1} \tag{32}$$

with t_s being the time constant of the angular acceleration estimation, which can be computed depending on the chosen gain settings of the angular acceleration complementary filter using $t_s = \frac{1}{\omega_{CF,\nu}}$.

D. Optimization-based control allocation

While operating at atmospheric altitudes, the GHGV-2 commands a redundant set of control surfaces (4 integrated flaps), which are used for the attitude control of the vehicle. Fig. 9 shows the available control effectors with the associated deflections of the upper left flap δ_{UL}, upper right flap δ_{UR}, lower left flap δ_{LL} and lower right flap δ_{LR}.

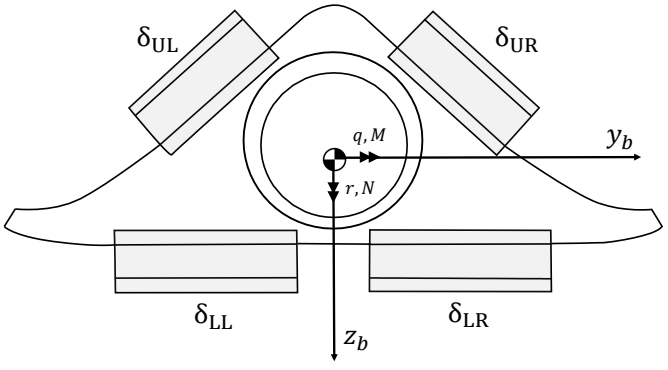

Fig. 9 Conceptual sketch with rear view of GHGV-2 and available control effectors during endoatmospheric operations [18].

The control effectiveness matrix B of the current operating point is required to solve the control allocation problem. The matrix describes the influences of all available control effectors on the balance of moment around the body-fixed axes of the aerial vehicle. In reality, such a matrix depends on a broad set of parameters, such as the current flight state, atmospheric conditions, and in some cases, the control inputs (e.g., due to cross-coupling). Nevertheless, to simplify the regarded problem, the last-mentioned dependency of the control effectiveness with regards to the control inputs itself is, in practice, often neglected, and hence a control affine dynamical system is assumed. In order to cope with the other mentioned nonlinear effects, the B matrix is constantly re-computed for each time step, using an OBPM and sensor information.

$$B = \begin{pmatrix} \frac{\partial L}{\partial \delta_{UL}} & \frac{\partial L}{\partial \delta_{UR}} & \frac{\partial L}{\partial \delta_{LL}} & \frac{\partial L}{\partial \delta_{LR}} \\ \frac{\partial M}{\partial \delta_{UL}} & \frac{\partial M}{\partial \delta_{UR}} & \frac{\partial M}{\partial \delta_{LL}} & \frac{\partial M}{\partial \delta_{LR}} \\ \frac{\partial N}{\partial \delta_{UL}} & \frac{\partial N}{\partial \delta_{UR}} & \frac{\partial N}{\partial \delta_{LL}} & \frac{\partial N}{\partial \delta_{LR}} \end{pmatrix} \tag{33}$$

$$\Delta\vec{\delta}^T = \begin{bmatrix} \Delta\delta_{UL} & \Delta\delta_{UR} & \Delta\delta_{LL} & \Delta\delta_{LR} \end{bmatrix}^T \tag{34}$$

The incrementalized control allocation problem can be solved for a simple case using a Moore-Penrose pseudoinverse. However, this approach implicitly neglects deflection limits $\Delta\vec{\delta}_{min/max}$ and rate limits $\Delta\dot{\vec{\delta}}_{min/max}$ of the control surfaces. Especially for highly nonlinear flight regimes in which control saturation could occur, that approach could reach its limits and could cause severe problems. Therefore it was decided to formulate the control allocation problem of the GHGV-2 as a constrained optimization problem. In this way, the mentioned operational constraints of the actuators can be considered. The resulting constrained optimization problem of the incrementalized control allocation algorithm can be stated as:

$$\begin{aligned} \underset{\Delta\vec{\delta} \in \mathbb{R}^{n_u}}{\arg\min} \quad & \|B\Delta\vec{\delta} - \Delta\vec{Q}_c\|_2 \\ \text{subject to} \quad & \Delta\vec{\delta}_{min} \le \Delta\vec{\delta} \le \Delta\vec{\delta}_{max}, \\ & \Delta\dot{\vec{\delta}}_{min} \le \Delta\dot{\vec{\delta}} \le \Delta\dot{\vec{\delta}}_{max} \end{aligned} \tag{35}$$

with n_u being the number of available control effectors. The least-squares optimization problem formulated here leads to the minimization of the difference between the requested incremental moment vector $\Delta\vec{Q}_c$ and the achievable incremental control input moment vector $B\Delta\vec{\delta}$ in the l_2 norm sense and with the incremental control deflection vector $\Delta\vec{\delta}$ complying with position and rate limits. The formulated optimization problem is solved using an active set algorithm that is based on a quadratic programming method in which the actuator limits are considered using Lagrange multipliers [24].

VI. Simulation results

A simulation-based analysis was carried out to examine the presented controller design. In the following analysis cases, different angle of attack commands α_{cmd} are given to the flight control system to assess the tracking performance for the following cases: nominal, in the presence of constant model uncertainties, and in the presence of sensor delay and noise.

The flight dynamics model and the applied aerodynamic data set used for the time simulations are provided in a MATLAB/Simulink environment developed for the control design of hypersonic flight vehicles; see [11] for more details. The integrated actuators of the employed control fins are modeled as second-order systems, which include preset deflection angle, rate, and acceleration limits. For the discussed assessment, the flight vehicle was trimmed at a selected operating point within the hypersonic speed regime and at a height band within the mesosphere.

A. Performance comparison for nominal case

The results for the assessment of the nominal model are shown in Fig. 10. The doublet reference command on α_{cmd} is shown in a dash-dotted black line, the filtered signal from the model reference system is shown as a dashed black line, and the response of the vehicle is displayed in a solid grey line.

It can be seen that the proposed controller adequately and smoothly tracks the delivered raw trajectory on the α_{cmd} channel with the desired response characteristics defined in the RM. Since no raw pitch rate command is given to the

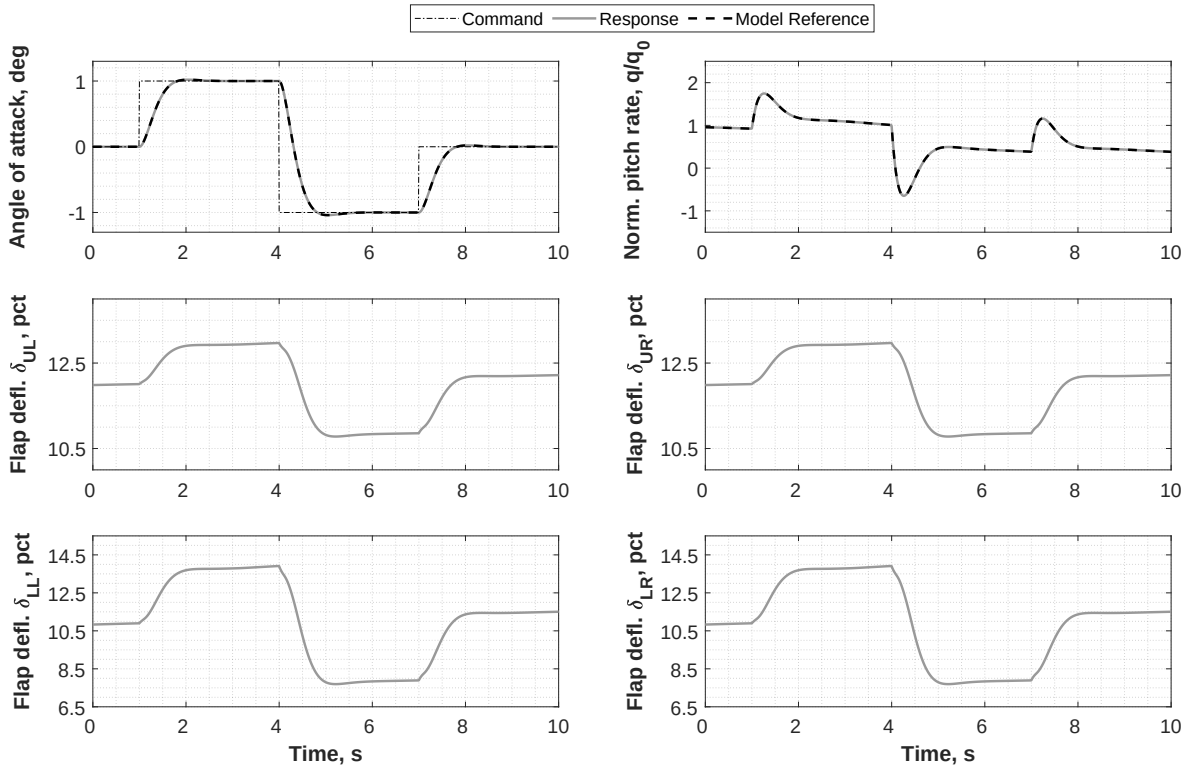

Fig. 10 Simulation results for a doublet command input on α_{cmd} in the nominal case. Displayed time series: angle of attack α in $^\circ$, normalized pitch rate in q/q_0 and flap deflections in % of the maximum deflection range. Dash-dotted black line: raw reference command, dashed black line: shaped reference signal, grey: vehicle response of closed-loop INMFC system

system, the shown shaped reference signal of the normalized pitch rate is computed using the $\dot{\alpha}_{ref}$ command of the RM. In order to compare it with a pitch rate in the body-fixed axis, the signal was transformed using the relationship presented in Eq. 17. The vehicle's normalized pitch rate closed-loop response follows the desired system behavior well and shows beneficial damping characteristics of the closed-loop system.

B. Performance comparison under the presence of model uncertainties

The following section examines the control performance and robustness of the proposed INMFC controller under the existence of model uncertainties. Further, the control performance and robustness are compared to a non-incremental control strategy (NMFC), for which the signals computed by Eq. (20) are not further incrementalized. To make the obtained results more meaningful for the reader and to show the benefits of the proposed incremental control strategy for both approaches, versions with additional integral controls on the α and q channel are studied and compared as well.

In the given analysis case, the regarded flight control systems were analyzed by inducing a unit step command into the flight control system's α_{cmd} channel under the presence of parametric model uncertainties. All compared control systems are using the same feedback design parameters $K_{\mu\alpha\beta}$ and K_{pqr} , as well as $K_{I,\alpha}$ and $K_{I,q}$ (for the cases in which integral controllers are included). Therefore, differences in the response can be only explained with effects coming from the incrementalization.

For this analysis it was decided to concentrate on the proposed controller's robustness assessment against static parametric uncertainties. The regarded model was modified in a way that static parameter deviations for $C_{m,0}$, $C_{m,\alpha}$ and the moment of inertia I are considered. For each as uncertain defined parameter a deviation of +40% from the nominal value was added to the simulation model.

The results for the described case are shown in Fig. 11. It can be observed that for the NMFC controller without integral controller, the model uncertainties would lead to a steady-state error in the response. However, when integral

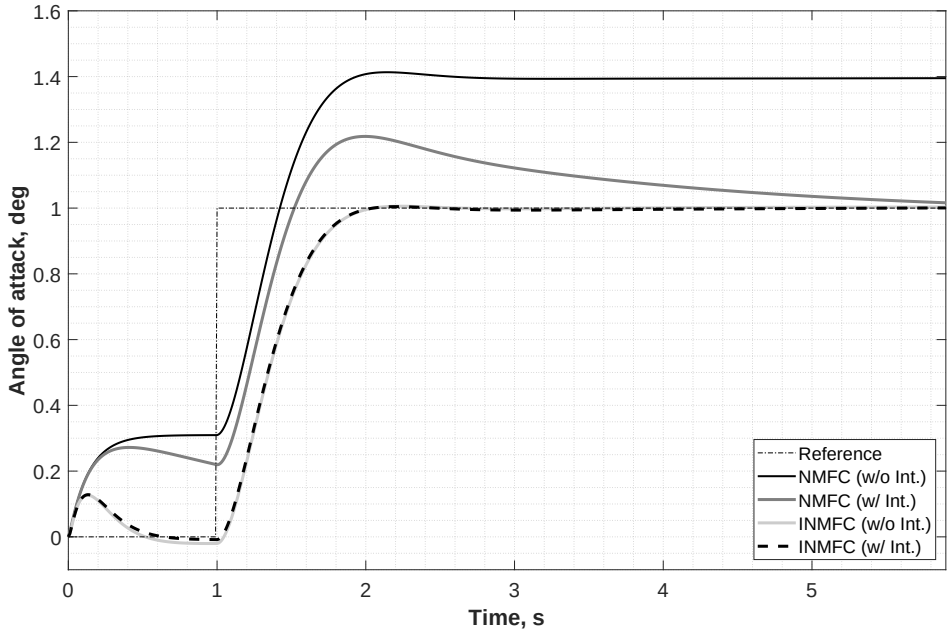

Fig. 11 Simulation results for a step command input on α_{cmd} in the case with static model uncertainties on $C_{m,0}$, $C_{m,\alpha}$ and I. Displayed time series: angle of attack α in °. Dash-dotted black line: reference command, solid black line: vehicle response for the closed-loop NMFC system without integral controller, solid dark grey line: vehicle response for the closed-loop NMFC system with integral controller, light grey line: vehicle response for the closed-loop INMFC system without integral controller, dashed black line: vehicle response for the closed-loop INMFC system with integral controller

controllers in both loops are added, the steady-state error converges to zero after a time period. The plots for the INMFC controller shows that the INMFC is better able to deal with model uncertainties. Further, it can be observed that both integral controllers have nearly no influence on the control performance of the INMFC system. This confirms some of the prior findings presented by Acquatella et al. in [9], in which the researchers have shown and discussed the similarities between incremental and integral control.

However, for completeness it needs to be stated that these uncertainties are part of an class of uncertainties that are noncritical for incremental control systems. Since possible uncertainties of those parameters are later substituted by sensor information, see [9] for further explanation. For incremental systems, the most influential uncertainties are uncertainties in the control effectiveness. These uncertainties are examined in an additional case for the INMFC without an integral system.

The model was modified such that the control effectiveness matrix B used in the simulation has a static parameter deviation +35% from the nominal value. The results for the assessment of the influence of an uncertain control effectiveness are shown in Fig. 11. It can be observed that the uncertainties on the control effectiveness are leading to a significant degradation of the closed-loop response. At the beginning of the simulation, the deviation leads to oscillations. Even though the system is able to damp those oscillations and converge to the desired reference state, it is assumed that for a more dynamic case, with continuous changes of the reference signal, the error would not converge to zero or, in the worst-case, the system would become unstable. This shows the need for an indirect adaptive control approach that is able to update the control effectiveness matrix B during the operation. An adaptive control architecture that can address the mentioned uncertainty is currently under investigation.

C. Performance comparison for case with sensor delay and noise

The following part highlights the tracking performance of the proposed INMFC architecture with degraded sensor information. In the given analysis case, the tracking performance is analyzed by inducing a varying reference signal into

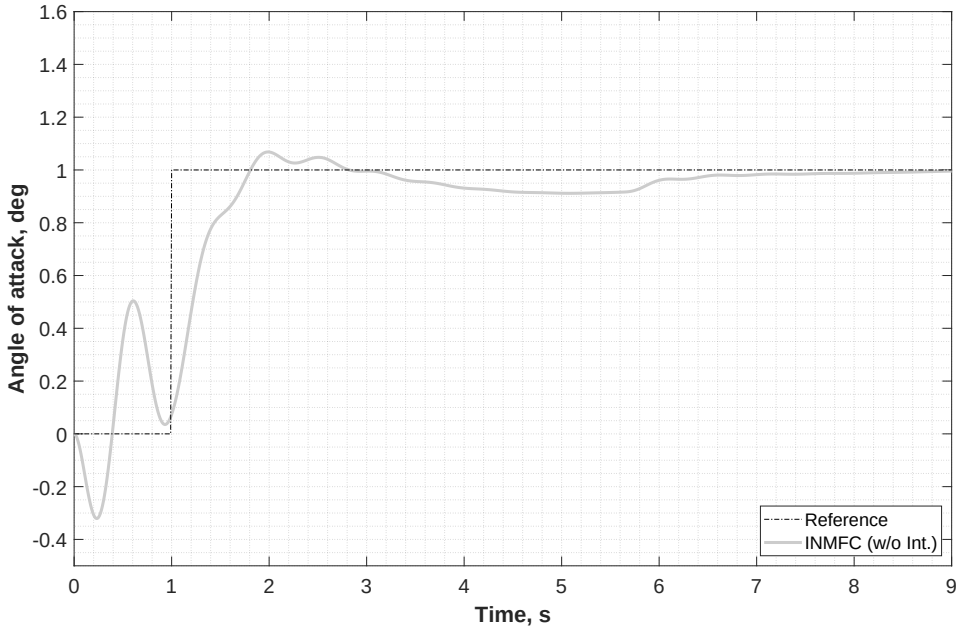

Fig. 12 Simulation results for a step command input on α_{cmd} in the case with static model uncertainties on the control effectiveness matrix B. Displayed time series: angle of attack α in °. Dash-dotted black line: reference command, grey: vehicle response for closed-loop INMFC system

the flight control system's α_{cmd} channel in the presence of sensor noise and time delays on the gyroscopic signal vector $(p, q, r)^T$. The gyroscopic signal vector was manipulated so that each element of the vector was augmented with a constant additive Gaussian white noise with a signal-to-noise ratio of 10 with respect to q_0 for this trim point. The constant time delay τ on the measurements was chosen as 0.05 sec.

Fig. 13 shows the results obtained from the described analysis. It can be noticed that the response of the control system is affected by the applied noise and time delays on the sensor information. However the system is still able to robustly follow the reference signal and suppress the signal noise in the response behavior of the vehicle.

VII. Conclusion

This paper presents an incremental nonlinear model following control architecture for the attitude control of an over-actuated conceptual hypersonic glide vehicle developed by DLR. The proposed flight control architecture applies a cascaded nonlinear dynamic inversion control methodology for feedback control and enhances the structures with a feedforward path based on nonlinear model following control. The methodology allows the command tracking tasks to be separated from the regulation tasks of the feedback control system and hence eases the tuning, and decreasing the possibility of high-gain solutions. The generated virtual control command is then incrementalized using a data fusion-based angular acceleration signal and later filtered control input information. The performance of the proposed control architecture was investigated in Sect. VI with longitudinal maneuvers for the nominal case and under the presence of aerodynamical uncertainties, as well as sensor and time delays. It was demonstrated that the proposed system handles the regarded system dynamics adequately in both investigated cases and provides good and robust tracking performance.

Acknowledgment

The author would like to thank and acknowledge all colleagues from DLR working within the HyBAB study for their contributions to the multidisciplinary design of the discussed vehicle. Special thanks go to Dr. Patrick Gruhn from the DLR Institute of Aerodynamics and Flow Technology for helpful discussions and for supporting the vehicle's high-fidelity modeling. Further, the author would like to thank Dr. Nicolas Fezans from the DLR Institute of Flight

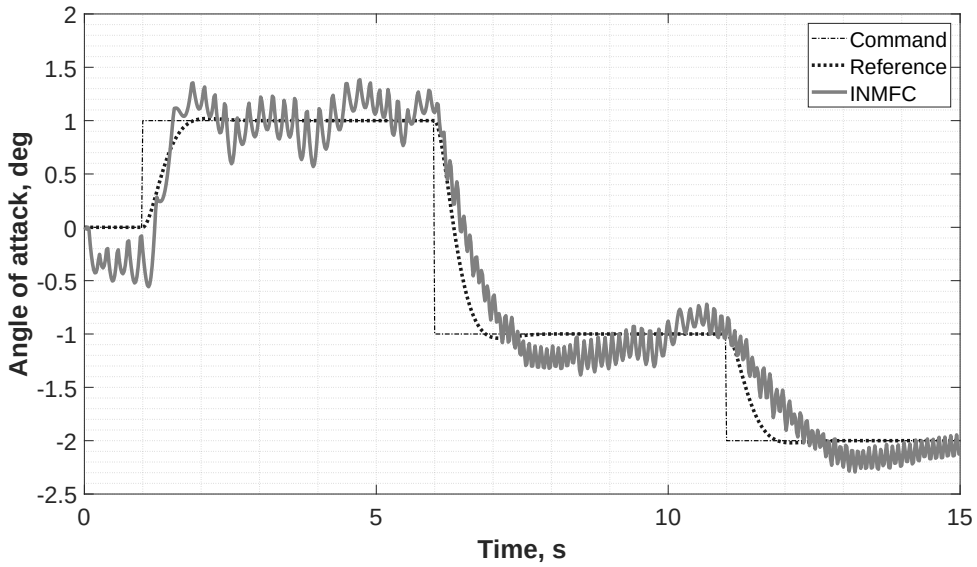

Fig. 13 Simulation results for a time varying command input on α_{cmd} with corrupted sensor information. Displayed time series: angle of attack α in $^\circ$. Dash-dotted black line: raw reference command, dashed black line: shaped reference signal, grey: vehicle response

Systems for fruitful conversations and suggestions within the field of flight dynamics and control.

References

[1] "Flight dynamics – Concepts, quantities and symbols – Part 1: Aircraft motion relative to the air," Standard, International Organization for Standardization (ISO), Geneva, Switzerland, Apr. 1988. ISO 1151-1:1988.

[2] "Flight dynamics – Concepts, quantities and symbols – Part 2: Motions of the aircraft and the atmosphere relative to the Earth," Standard, International Organization for Standardization (ISO), Geneva, Switzerland, Sep. 1985. ISO 1151-2:1985.

[3] Rollins, E., Valasek, J., Muse, J., and Bolender, M., "Nonlinear Adaptive Dynamic Inversion Applied to a Generic Hypersonic Vehicle," *AIAA Guidance, Navigation, and Control (GNC) Conference*, Boston, Massachusetts, US, 2007. https://doi.org/10.2514/6.2013-5234, URL https://arc.aiaa.org/doi/abs/10.2514/6.2013-5234.

[4] Breitsamter, C., Cvrlje, T., Laschka, B., Heller, M., and Sachs, G., "Lateral-Directional Coupling and Unsteady Aerodynamic Effects of Hypersonic Vehicles," *Journal of Spacecraft and Rockets*, Vol. 38, No. 2, 2001, pp. 159–167. https://doi.org/10.2514/2.3689, URL https://doi.org/10.2514/2.3689.

[5] Bolender, M., and Doman, D., "Nonlinear Longitudinal Dynamical Model of an Air-Breathing Hypersonic Vehicle," *Journal of Spacecraft and Rockets*, Vol. 44, 2007, pp. 374–387. https://doi.org/10.2514/1.23370.

[6] Preller, D., and Smart, M. K., "Longitudinal Control Strategy for Hypersonic Accelerating Vehicles," *Journal of Spacecraft and Rockets*, Vol. 52, No. 3, 2015, pp. 993–999. https://doi.org/10.2514/1.A32934, URL https://doi.org/10.2514/1.A32934.

[7] da Costa, R. R., Chu, Q. P., and Mulder, J. A., "Reentry Flight Controller Design Using Nonlinear Dynamic Inversion," *Journal of Spacecraft and Rockets*, Vol. 40, No. 1, 2003, pp. 64–71. https://doi.org/10.2514/2.3916, URL https://doi.org/10.2514/2.3916.

[8] Lee, H., Reiman, S., Dillon, C., and Youssef, H., "Robust Nonlinear Dynamic Inversion Control for a Hypersonic Cruise Vehicle," *AIAA Guidance, Navigation and Control Conference and Exhibit*, Hilton Head, South Carolina, US, 2007. https://doi.org/10.2514/6.2007-6685, URL https://arc.aiaa.org/doi/abs/10.2514/6.2007-6685.

[9] Acquatella, P., Falkena, W., van Kampen, E.-J., and Chu, Q. P., "Robust Nonlinear Spacecraft Attitude Control using Incremental Nonlinear Dynamic Inversion." *AIAA Guidance, Navigation, and Control Conference*, Minneapolis, Minnesota, US, 2012. https://doi.org/10.2514/6.2012-4623, URL https://arc.aiaa.org/doi/abs/10.2514/6.2012-4623.

[10] Pfeifle, O., and Fichter, W., "Cascaded Incremental Nonlinear Dynamic Inversion for Three-Dimensional Spline-Tracking with Wind Compensation," *Journal of Guidance, Control, and Dynamics*, Vol. 44, No. 8, 2021, pp. 1559–1571. https://doi.org/10.2514/1.G005785, URL https://doi.org/10.2514/1.G005785.

[11] Autenrieb, J., Fezans, N., Gruhn, P., and Klevanski, J., "Towards a Control-Centric Modelling and Simulation-Framework for Hypersonic Glide Vehicles," *German Aeronautics and Space Congress (DLRK)*, Bremen, Germany, 2021.

[12] Gruhn, P., "Design and Analysis of a Hypersonic Glide Vehicle (Original German Title: Auslegung und Analyse eines hypersonischen Gleitflugkörpers)," *Conference on Applied Research for Defense and Security in Germany*, Bonn, Germany, 2020.

[13] Chai, R., Tsourdos, A., Savvaris, A., Chai, S., and Xia, Y., "Trajectory planning for hypersonic reentry vehicle satisfying deterministic and probabilistic constraints," *Acta Astronautica*, Vol. 177, 2020, pp. 30–38. https://doi.org/https://doi.org/10.1016/j.actaastro.2020.06.051, URL https://www.sciencedirect.com/science/article/pii/S0094576520304203.

[14] Gerhold, T., "Overview of the Hybrid RANS Code TAU," *MEGAFLOW - Numerical Flow Simulation for Aircraft Design*, edited by N. Kroll and J. K. Fassbender, Springer Berlin Heidelberg, Berlin, Heidelberg, 2005, pp. 81–92. https://doi.org/10.1007/3-540-32382-1_5.

[15] Gerhold, T., "Overview of the Hybrid Rans Code TAU," *Notes on Numerical Fluid Mechanics and Multidisciplinary Design*, Vol. 89, 2002. https://doi.org/10.1007/3-540-32382-1_5.

[16] Kiehn, D., "Stability Analysis and Flight Control Design of the Winged Reusable Launch Vehicle ReFEx," *CEAS Space Journal*, Vol. 13, 2020. https://doi.org/10.1007/s12567-020-00319-3.

[17] Snell, S. A., and Enns, W. L., F. D.and Garrard, "Nonlinear Inversion Flight Control for a Supermaneuverable Aircraft," *Journal of Guidance, Control, and Dynamics*, Vol. 15, No. 4, 1992, pp. 976–984. https://doi.org/10.2514/3.20932, URL https://doi.org/10.2514/3.20932.

[18] Autenrieb, J., and Fezans, N., "Nonlinear Model Following Control Design for a Hypersonic Waverider Configuration," *CEAS EuroGNC "Conference on Guidance, Navigation and Control", 3–5 May 2022, TU Berlin, Germany*, 2022.

[19] Wang, M., Zhang, S., Holzapfel, F., and Zhang, F., "Backup Controller for Large Transport Aircraft with Insufficient Natural Stability," *Journal of Guidance, Control, and Dynamics*, Vol. 40, No. 3, 2017, pp. 666–679. https://doi.org/10.2514/1.G002202, URL https://doi.org/10.2514/1.G002202.

[20] Grondman, F., Looye, G., Kuchar, R. O., Chu, Q. P., and Kampen, E.-J. V., "Design and Flight Testing of Incremental Nonlinear Dynamic Inversion-based Control Laws for a Passenger Aircraft," *2018 AIAA Guidance, Navigation, and Control Conference*, Kissimmee, Florida, US, 2018. https://doi.org/10.2514/6.2018-0385, URL https://arc.aiaa.org/doi/abs/10.2514/6.2018-0385.

[21] Jiali, Y., and Jihong, Z., "An angular acceleration estimation method based on the complementary filter theory," *2016 IEEE International Instrumentation and Measurement Technology Conference Proceedings*, Taipei, Taiwan, 2016, pp. 1–6. https://doi.org/10.1109/I2MTC.2016.7520548.

[22] Higgins, W. T., "A Comparison of Complementary and Kalman Filtering," *IEEE Transactions on Aerospace and Electronic Systems*, Vol. AES-11, No. 3, 1975, pp. 321–325. https://doi.org/10.1109/TAES.1975.308081.

[23] Sieberling, S., Chu, Q. P., and Mulder, J. A., "Robust Flight Control Using Incremental Nonlinear Dynamic Inversion and Angular Acceleration Prediction," *Journal of Guidance, Control, and Dynamics*, Vol. 33, No. 6, 2010, pp. 1732–1742. https://doi.org/10.2514/1.49978, URL https://doi.org/10.2514/1.49978.

[24] Härkegård, O., "Dynamic Control Allocation Using Constrained Quadratic Programming," *Journal of Guidance Control and Dynamics*, Vol. 27(6), 2004. https://doi.org/10.2514/1.11607.